

## Article

# Prediction of Soil Moisture Content from Sentinel-2 Images Using Convolutional Neural Network (CNN)

Ehab H. Hegazi <sup>1,2</sup> , Abdellateif A. Samak <sup>2</sup>, Lingbo Yang <sup>3</sup>, Ran Huang <sup>3</sup>  and Jingfeng Huang <sup>1,4,\*</sup> 

<sup>1</sup> Institute of Applied Remote Sensing and Information Technology, Zhejiang University, Hangzhou 310058, China

<sup>2</sup> Agricultural and Biosystem Engineering Department, Faculty of Agriculture, Menoufia University, Shebin EL-Kom 32511, Egypt

<sup>3</sup> School of Artificial Intelligence, Hangzhou Dianzi University, Hangzhou 310018, China

<sup>4</sup> Key Laboratory of Environmental Remediation and Ecological Health, Ministry of Education, Zhejiang University, Hangzhou 310058, China

\* Correspondence: hjf@zju.edu.cn; Tel.: +86-571-8898-2830

**Abstract:** Agriculture is closely associated with food and water. Agriculture is the first source of food but the biggest consumer of freshwater. The population is constantly increasing. Smart agriculture is one of the means of achieving food and water security. Smart agriculture can help improve water management and increase agricultural production, thus counteracting rapid population growth requirements. Soil moisture estimation is a critical step in agricultural water management. Soil moisture measurement techniques in situ are point measurements, labor-intensive, time-consuming, tedious, and expensive. We propose, in this research, a new approach to predict soil moisture over vegetation-covered areas from Sentinel-2 images based on a convolutional neural network (CNN). CNN architecture (3) consisting of six convolutional layers, one pooling layer, and two fully connected layers has achieved the highest prediction accuracy. Three well-known criteria including coefficient of determination ( $R^2$ ), mean absolute error (MAE), and root mean square error (RMSE) are utilized to measure the accuracy of the proposed algorithm. The Red Edge 3, NIR, and SWIR 1 are the most appropriate Sentinel-2 bands for retrieving soil moisture in vegetation-covered areas. Normalized Difference Water Index (NDWI) and Normalized Difference Vegetation Index (NDVI) are the best indicators. The use of the indicator is more proper than the use of the single Sentinel-2 band as input data for the proposed CNN architecture for predicting soil moisture. However, using combinations “that consist of some number of Sentinel-2 bands” as input data for CNN architecture is better than using each indicator separately or all of them as a group. The best values of the performance metrics were achieved using the sixth combination ( $R^2 = 0.7094$ , MAE = 0.0277, RMSE = 0.0418) composed of the Red, Red Edge 1, Red Edge 2, Red Edge 3, NIR, and Red Edge 4 bands as input data to the CNN architecture (3), as well as by using the fifth combination ( $R^2 = 0.7015$ , MAE = 0.0287, RMSE = 0.0424) composed of the Red Edge 3, NIR, Red Edge 4, and SWIR 1 bands.

**Keywords:** smart agriculture; remote sensing; soil moisture content; Sentinel-2; Google Earth Engine; artificial intelligence; convolutional neural network



**Citation:** Hegazi, E.H.; Samak, A.A.; Yang, L.; Huang, R.; Huang, J. Prediction of Soil Moisture Content from Sentinel-2 Images Using Convolutional Neural Network (CNN). *Agronomy* **2023**, *13*, 656. <https://doi.org/10.3390/agronomy13030656>

Academic Editors: Dimitrios D. Alexakis and Gniewko Niedbała

Received: 19 December 2022

Revised: 7 February 2023

Accepted: 22 February 2023

Published: 24 February 2023



**Copyright:** © 2023 by the authors. Licensee MDPI, Basel, Switzerland. This article is an open access article distributed under the terms and conditions of the Creative Commons Attribution (CC BY) license (<https://creativecommons.org/licenses/by/4.0/>).

## 1. Introduction

The world population is constantly increasing and, in 2050, is expected to reach about 9.725 billion [1]. The agricultural sector is the major contributor of the production of the food that people eat [2]. With the growth in the global population, annual world agricultural production in 2050 is supposed to be 60 percent higher than it was in 2005 [3], which will intensify pressures on natural resources [4]. Global food production depends on the availability of water [5]. Under future climate conditions, global food production is projected to decrease [6]. In the future, the intensifying competition for water resources

is projected to increase [7]. Hence, increasing agricultural production simultaneously with achieving the optimal use of water resources is considered vital to feed and drink 9.725 billion in the future.

Agriculture is the largest consumer of water around the world, at 70 percent of all freshwater withdrawals [8]. Agricultural water-use efficiency can be increased by optimizing irrigation scheduling [9]. Irrigation scheduling aims to determine and apply the exact amount of water at the perfect time [10]. Irrigation scheduling techniques depend on soil moisture measurements [11]. Soil moisture usually refers to the amount of water stored in the upper centimeters of soil [12] and is spatially and temporally highly variable [13]. Soil moisture strongly impacts plant growth and hence agricultural productivity [14]. Soil moisture estimation is necessary for accurate irrigation water management [15]. Gravimetric, neutron probe, time-domain reflectometer (TDR), frequency domain reflectometer (FDR), and tensiometer methods are the most commonly used to estimate the soil moisture content in situ [16]. Traditional in situ soil moisture measurement methods possess relatively high precision, but the spatial representativeness for point-based measurements is limited [17]. Furthermore, implementing such methods is destructive, costly, and labor-intensive [18].

Satellite remote sensing of soil moisture is vital and significant [19]. A good deal of research work has been conducted on the electromagnetic spectrum from the optical to the microwave region; as a result, researchers have developed several remote sensing methods for investigating soil moisture [20]. Optical methods are especially valuable for the remote sensing of soil moisture since the reflected solar radiation is the strongest passive signal available to satellites [21]. The spectral reflectance decreases with increasing soil moisture [22]. Ref. [23] utilized MODIS data to retrieve soil moisture content at a depth of 20 cm in Sanjiang Plain, China ( $R^2$  ranged from 0.10 to 0.50). Ref. [24] successfully estimated the soil moisture (0–20 cm) using Landsat data. Based on Landsat 8 data, Ref. [25] developed two indices to estimate soil moisture at a depth of 20 cm, the Triangle Soil Moisture Index ( $R = 0.57$ ,  $RMSE = 0.084$ ) and the Modified Triangle Soil Moisture Index ( $R = 0.65$ ,  $RMSE = 0.087$ ). Ref. [26] used a linear regression model to determine surface soil moisture (0–20 cm) from Landsat 8 satellite images ( $R^2 = 0.564$ ). In optical remote sensing, the short-wave infrared (SWIR) bands are better suited for monitoring soil moisture than the visible and NIR bands [21,27,28]. The SWIR 1 band is more sensitive than the SWIR 2 band for plants and soil moisture content [29], while Ref. [30] mentioned that the SWIR 2 band is better than the SWIR 1 band for describing soil moisture contents. High-resolution Sentinel-2 optical images are a good data source for estimating soil moisture ( $r = 0.80$ ) over agricultural areas and thus support farm managers in decision-making on irrigation scheduling [31]. Ma et al. [32] proposed an algorithm to retrieve soil moisture content from Sentinel-1 and Sentinel-2 data over vegetation-covered regions, wherein  $R^2$  ranged from 0.472 to 0.665 and RMSE ranged from 0.039 to 0.078. Using an artificial neural network (ANN), Ref. [33] developed an approach to estimate soil moisture based on Sentinel-1 and Sentinel-2 data, and the accuracy of soil moisture estimation ranged from ( $R = 0.307$ ,  $RMSE = 0.095$ ) to ( $R = 0.785$ ,  $RMSE = 0.062$ ). Sentinel-2 data are more suitable for retrieving soil moisture over wheat-covered areas [34]. Using the random forest regression algorithm, the use of all Sentinel-2 bands achieved the highest coefficient of determination and the lowest RMSE by comparison to the use of individual bands [35]. Sentinel-2 bands are proper to retrieve soil moisture; the coefficients of determination ( $R^2$ ) for Blue, Green, Red, NIR, SWIR 1, and SWIR 2 are 0.191, 0.493, 0.575, 0.600, 0.732, and 0.738, respectively [36]. Red Edge bands are the most sensitive for estimating soil moisture in vegetation-covered areas, followed by the SWIR bands [37]. The Red Edge 1, Red Edge 2, Red Edge 3, NIR, and Red Edge 4 bands are suitable for land moisture mapping [29]. In vegetation-covered areas, using Red Edge bands improve the soil moisture estimation accuracy [37]. Vegetation water content is a significant parameter in retrieving soil moisture from satellite imagery [38,39]. One effective method for the retrieval of vegetation water content is the combination of near-infrared (NIR) and short-wave infrared (SWIR) bands [40]. Several indices are based on the NIR and SWIR bands [41–44]. NIR

and SWIR bands are proper for soil moisture prediction [45]. Based on the NIR-Red spectral space, [46] developed a new simple method for soil moisture monitoring, and [25] introduced two effective and real-time soil moisture indices. Google Earth Engine (GEE) is a computing platform developed and designed to enable and empower everyone to use Google's massive computational capabilities [47]. GEE is an indispensable source for the acquisition and processing of satellite images [48].

Artificial intelligence is one of the fields of computer science that aims at simulating human intelligence processes [49]. Machine learning is a branch of artificial intelligence [50] capable of extracting knowledge from big data [51]. Machine learning aims to develop algorithms that can automatically learn, improve, and generalize from a given set of examples, in order to make predictions or decisions without being explicitly programmed to do so [52]. Deep learning is a class of machine learning algorithms [53]. Convolutional neural network (CNN) is one of the most popular classes of deep learning methods [54]. CNN architecture comprises an input data layer, one or more hidden layers, and an output data layer [55]. Commonly, hidden layers of a CNN consist of convolutional layers, pooling layers, normalization layers, and fully connected layers [56]. CNN performs well in unstructured data and achieves good results [57]. A CNN has a powerful ability for automatic feature extraction [58]. CNN has achieved great success in soil moisture retrieval accuracy ( $R^2 = 0.8664$ ) over agricultural areas from Sentinel-1 images [19].

As a result of the former review, accurate soil moisture estimation is a prerequisite for achieving proper irrigation water management. The most common disadvantages of in-situ soil moisture measurement methods are that they are: point measurements, labor-intensive, time-consuming, tedious, and expensive. Thus, the present research aims to provide a new approach for remotely sensing the moisture content in the soil. The main goal of our proposed approach is the integration of artificial intelligence techniques and satellite imagery data to serve the agricultural sector. In the present work, we propose CNN architecture for predicting or estimating soil moisture (0–20 cm) from Sentinel-2 images.

## 2. Materials and Methods

### 2.1. Study Field Description and Data Collection

In-situ soil moisture observations are necessary to build and validate the soil moisture prediction model. The International Soil Moisture Network (ISMN) is a global open-source database for in situ soil moisture data (<https://ismn.geo.tuwien.ac.at/en/> (accessed on 9 July 2022)). ISMN includes multiple networks distributed around the world. ISMN is a suitable means for validating and improving algorithms for soil moisture retrieval from Satellite images [59,60]. In this study, we utilized in-situ soil moisture data of the OzNet and WegenerNet networks from 28 March 2017 to 1 November 2020.

OzNet is a hydrological monitoring network established within the Murrumbidgee River catchment in South-Eastern Australia. The location of the Murrumbidgee catchment has significant spatial variability in the climate (ranging from semiarid to humid), the texture of soil (ranging from sandy to clayey), and land use (dryland farming, irrigated farming, remnant vegetation, and urban areas). This catchment comprises 38 soil moisture-monitoring stations, with a concentration of sites in three subareas: Kyeamba Creek, Adelong Creek, and Yanco Region. Three Campbell Scientific water content reflectometers (CS615, CS616, and Stevens Hydra Probe) were installed at stations to measure in-situ soil moisture. Moreover, Time Domain Reflectometry (TDR) probes were installed and used to calibrate the reflectometers. Soil moisture was continuously measured and recorded every 20 min at three depths (0–30, 30–60, and 60–90 cm). Plus, each station measures air temperature, soil temperature, soil suction, precipitation, wind speed, relative humidity, and ancillary data. Only 17 soil moisture-monitoring stations were selected and used in this study, 6 in Kyeamba Creek and 11 in Yanco Region. For more detailed information on the OzNet network, see [61,62]. The OzNet network data are freely accessible via (<http://www.oznet.org.au/> (accessed on 9 July 2022)).

WegenerNet Feldbach Region is a high-resolution meteorological observation network established within the Feldbach region in South-Eastern Styria, Austria. The climate in Feldbach is affected by both continental and Mediterranean climates. Winters are cold, whereas summers are hot and rainy. The main land uses in the Feldbach region are agriculture and forestry. WegenerNet Feldbach Region network comprises 155 stations within a limited area of approximately  $22 \times 16$  km. This network includes 12 soil moisture-monitoring stations: Stations No. 6, 15, 19, 27, 34, 50, 54, 77, 78, 84, 85, and 99. The dominant soil type for all station sites is sandy loam, except for station No. 19, where the soil type is silty clay. Inside each station, Stevens Hydra Probe II was used to measure soil moisture at a depth of 0–20 cm. In addition, each station measures relative humidity, air temperature, diode temperature, precipitation, pF-value, soil temperature, soil conductivity, and ancillary data. All data of the WegenerNet network are freely accessible via (<http://www.wegenernet.org/> (accessed on 9 July 2022)). We used level 2 half-hourly data version 7 in this study. Additional information and a detailed explanation of the WegenerNet Feldbach Region network are provided in [63–65]. Figure 1 shows the locations of the OzNet and WegenerNet stations used in the present research. In this research, the surface measurements, 0–30 cm at OzNet Network and 0–20 cm at WegenerNet Network, were considered only as input (Y-values) for modeling the soil moisture content.

## 2.2. Sentinel-2 Imagery and Pre-Processing

Retrieving soil moisture over vegetation-covered areas from Sentinel-2 images is the main objective of this research. Sentinel-2 optical mission comprises a constellation of two identical satellites, Sentinel-2A and Sentinel-2B. Sentinel-2A was launched on 23rd June 2015, while Sentinel-2B was launched on 7th March 2017. The launch of Sentinel-2A and Sentinel-2B helped to halve revisit time from 10 to 5 days. Depending on the spectral band, the spatial resolutions of Sentinel-2 data are 10, 20, and 60 m. Sentinel-2 satellite provides multi-spectral data with 13 spectral bands, as highlighted in Table 1. All these bands were used in this study: except Band 1 (Aerosols), Band 9 (Water Vapor), and Band 10 (SWIR-Cirrus), as these bands are dedicated mainly to atmospheric corrections and cloud screening [66]. All the Sentinel-2 data used in this study are Level-2A products, which means per-pixel radiometric measurements are provided in surface reflectance with all parameters to transform them into radiances. Google Earth Engine (GEE) is a free platform (<https://earthengine.google.com/> (accessed on 13 September 2022)). GEE provides online access to Sentinel-2 level-2A data that is pre-processed using Sen2Cor. Level-2A processing comprises a scene classification and an atmospheric correction applied to Level-1C orthoimage products [67,68].

**Table 1.** Sentinel-2 spectral bands.

Band	Description	Center Wavelength (nm)	Bandwidth (nm)	Spatial Resolution (m)
B1	Aerosols	443	20	60
B2	Blue	490	65	10
B3	Green	560	35	10
B4	Red	665	30	10
B5	Red Edge 1	705	15	20
B6	Red Edge 2	740	15	20
B7	Red Edge 3	783	20	20
B8	NIR	842	115	10
B8a	Red Edge 4	865	20	20
B9	Water Vapor	945	20	60
B10	SWIR-Cirrus	1380	30	60
B11	SWIR 1	1610	90	20
B12	SWIR 2	2190	180	20

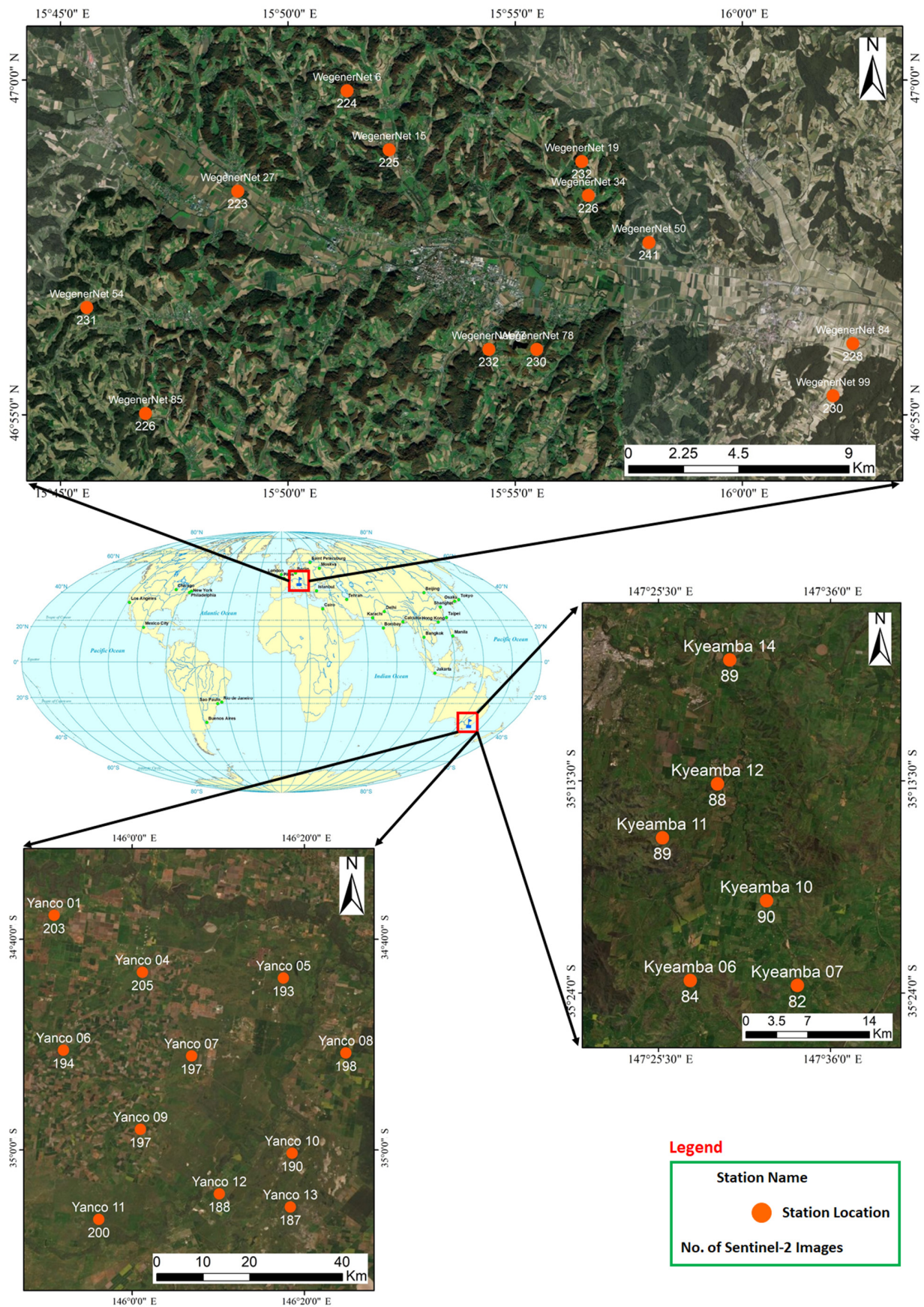


**Figure 1.** Map of soil moisture stations used during this study and the number of Sentinel-2 images available for each station location.

The current study included 29 soil moisture-monitoring stations. Each ground station covers a small area of land compared to the area covered by the Sentinel-2 image. In ArcGIS, we created a shapefile for each station separately. The shapefile is square, and the center of this shapefile is the installation position of the soil moisture sensor. All shapefiles are of the same size. Therefore, the downloaded Sentinel-2 images have the same volume ( $32 \times 32 \times 10$ ), where 32 represents the height (Rows), 32 represents the width (Columns), and 10 represents the Sentinel-2 bands (Channels). Every Sentinel-2 image consists of ten bands: Blue, Green, Red, Red Edge 1, Red Edge 2, Red Edge 3, NIR, Red Edge 4, SWIR 1, and SWIR 2. Using the created shapefiles, the total number of Sentinel-2 images downloaded from GEE is 5422 images, as shown in Figure 1. Now, the images are ready for training and testing are: Sentinel-2 images (X-values) and in-situ soil moisture (Y-values).

### 2.3. Establishment and Evaluation of the CNN Prediction Model

Convolutional neural network (CNN) is a widely used tool in research domains. CNN has the potential to analyze and understand satellite images. The proposed CNN architecture comprises an image input layer, hidden layers, and an output layer. Hidden layers contain convolutional, nonlinearity, pooling, and fully connected layers. The convolutional layer is mainly responsible for automatic feature extraction. The nonlinearity layer in a CNN applies element-wise nonlinearity using an activation function. Activation functions play a crucial role in the performance of a convolutional neural network. CNN allows using different activation functions for each layer. The proper choice of activation function improves the ability of the CNN model to learn the training dataset, hence the learning efficiency. The activation functions used in this study are: tanh, sigmoid, relu, and linear. The pooling layer aims to decrease the input image size and only keep the most significant features. The outputs of convolutional and pooling layers are the inputs for the fully connected layers. Flatten layer is needed between the convolutional or pooling layers and the fully connected layers to transform the data into a one-dimensional (1D) array of numbers. Fully connected layers, also call as dense layers, connect every neuron in one layer to every neuron in the next layer. Finally, the final layer is the output layer and has one neuron with a sigmoid activation function. For more detailed information about the design of CNN architectures, see [69,70].

Our overarching objective in this paper is to provide a CNN architecture able to retrieve or predict soil moisture with high accuracy and high efficiency from Sentinel-2 images. Identifying the best-performing architecture is an important step but the hardest. We designed three CNN architectures of different sizes in this study, as illustrated in Figure 2. In the three architectures (1, 2, and 3), pooling and fully connected layers are the same. The main differences between CNN architectures are the number of both convolutional layers and convolutional filters. The proper choice of activation functions can improve the performance of the CNN architecture for prediction. For this reason, we have done several experiments and tests to choose the best. Activation functions shown in Figure 2 were best suited for this type of data.

In general, the prediction accuracy of the algorithm depends on inputs and selecting the proper algorithm for these inputs. CNN is an appropriate technique for unstructured data types. CNN has great potential for automatic feature extraction. Hence, selecting and determining the best inputs is a crucial step in achieving the highest prediction accuracy. In this study, we first need to identify the impact of using Sentinel-2 bands as input data for CNN on soil moisture retrieval. Further, several indices derived from optical observations are used extensively for retrieving soil moisture. The most common are: Normalized Difference Vegetation Index ( $NDVI = (NIR - Red) / (NIR + Red)$ ) [71], Global Vegetation Moisture Index ( $GVMi = ((NIR + 0.1) - (SWIR 2 + 0.02)) / ((NIR + 0.1) + (SWIR 2 + 0.02))$ ) [41,44], and Normalized Difference Water Index ( $NDWI = (NIR - SWIR 1) / (NIR + SWIR 1)$ ) [42,43]. We, therefore, need to explore the influence of these indices on soil moisture retrieval. Third, we made several new combinations of Sentinel-2 bands, attempting to know the effect of using these combinations on soil moisture retrieval efficiency.

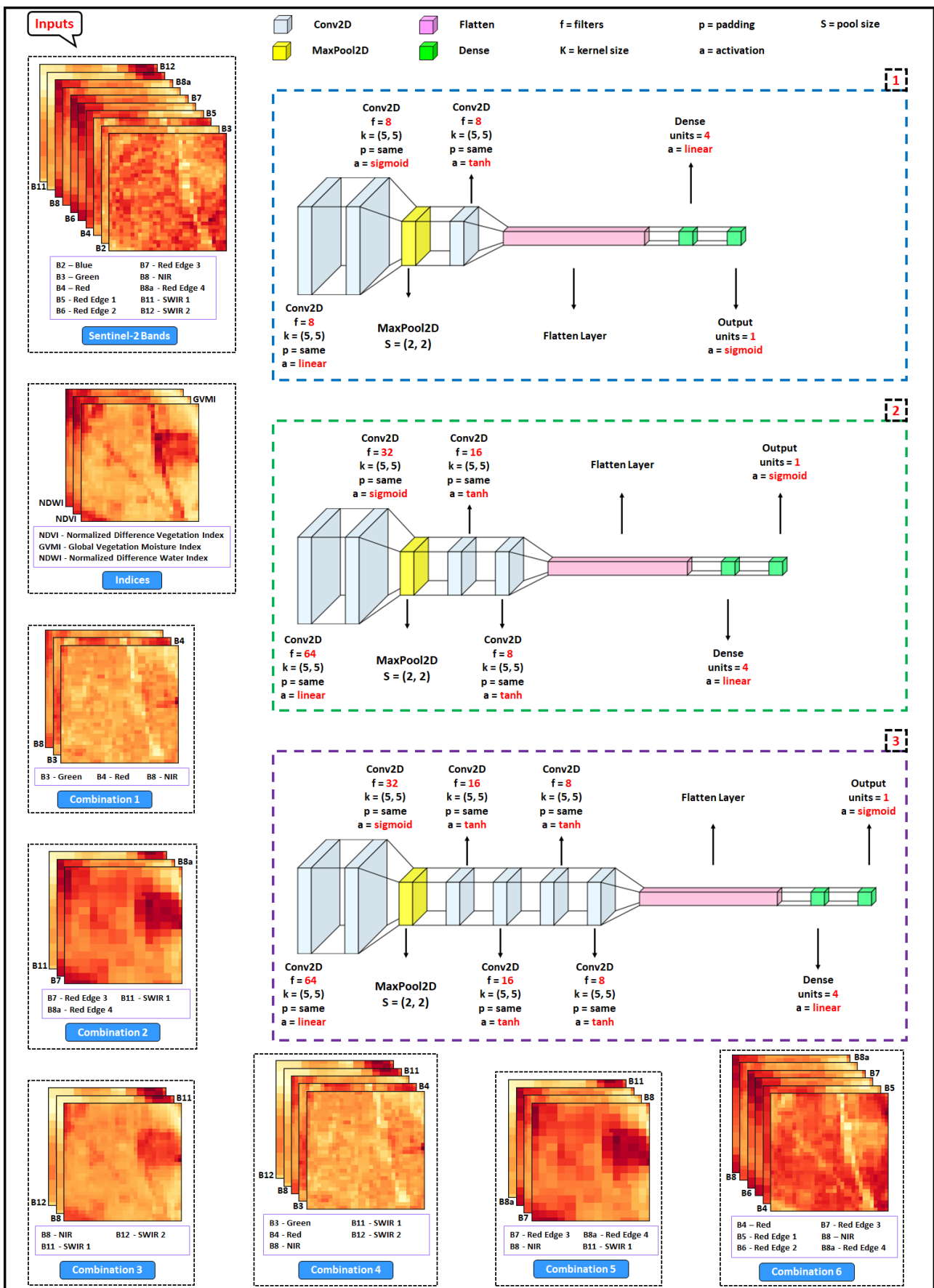


Figure 2. An illustration of Convolutional Neural Network (CNN) architectures.

The total number of Sentinel-2 images used to run the CNN model is 5422. In practice, we randomly split the dataset into two parts for fitting the model: 80% training set and 20% test set. In this study, we implemented the proposed CNN algorithm with Python programming language. The prediction accuracy of the CNN algorithm was measured using the coefficient of determination ( $R^2$ ), mean absolute error (MAE), and root mean square error (RMSE). The following equations illustrate these measures:

$$R^2 = 1 - \frac{\sum_{i=1}^n (y_i - \hat{y}_i)^2}{\sum_{i=1}^n (y_i - \bar{y})^2}$$

$$MAE = \frac{1}{n} \sum_{i=1}^n |y_i - \hat{y}_i|$$

$$RMSE = \sqrt{\frac{1}{n} \sum_{i=1}^n (y_i - \hat{y}_i)^2}$$

where ( $n$ ) is the number of datasets, ( $y_i$ ) is the actual value, ( $\hat{y}_i$ ) is the predicted value of ( $y_i$ ), and ( $\bar{y}$ ) is the mean of the ( $y$ ) values.

The modeling process was performed on a Windows workstation (Windows 10) with Intel Xeon Gold 5218 Processors (16-Cores, 16M Cache), 128 GB of RAM, and NVIDIA Quadro P4000 graphics cards (8 GB of RAM).

### 3. Results and Discussion

A comparison between CNN architecture (1), CNN architecture (2), and CNN architecture (3) indicated that CNN architecture (3) is the most suitable for Sentinel-2 data, as will be seen later in this paper. We, therefore, suffice with presenting the results of CNN architecture (3).

#### 3.1. Influence of Using Sentinel-2 Bands

Figure 3 summarizes the results of using Sentinel-2 bands as input data for CNN algorithm (CNN architecture (3)) on soil moisture retrieval accuracy. Scatter plots in the figure illustrate relations between in-situ soil moisture and predicted soil moisture by the proposed CNN algorithm. Initially, each band separately was used as input data for the CNN, and then all Sentinel-2 bands together (10 bands) were used.

All in all, we noticed that Sentinel-2 bands have a significant positive effect on soil moisture retrieval. The largest of them was the Red Edge 3 band, but the smallest of them was the Blue band. The coefficients of determination ( $R^2$ ) for Blue, Green, Red, Red Edge 1, Red Edge 2, Red Edge 3, NIR, Red Edge 4, SWIR 1, and SWIR 2 were 0.5192, 0.5425, 0.5796, 0.5458, 0.5664, 0.6098, 0.5967, 0.5877, 0.6093, and 0.5829, respectively. With the use of all Sentinel-2 bands as input data to the CNN model, the values of performance metrics manifestly improved ( $R^2 = 0.6799$ , MAE = 0.0282, RMSE = 0.0439).

The obtained results showed that the SWIR 1 band is more sensitive than visible and NIR bands for estimating soil moisture. This result is in agreement with the results reported by [21,27,28]. Further, the SWIR 1 band is better suited than the SWIR 2 band for determining soil moisture contents. This result is in agreement with [29] but is in disagreement with [30]. Red Edge 3, followed by SWIR 1, and then NIR are suitable bands for estimating soil moisture in vegetation-covered areas. This result is similar to the result found by [37]. The least sensitive band to retrieve soil moisture is Blue. This result is similar to the observation of [36]. Using all Sentinel-2 bands as input data to the CNN model is better than using individual Sentinel-2 bands for retrieving soil moisture from Sentinel-2 images. This result is consistent with the results of [35], who showed that the use of all Sentinel-2 bands achieved a prediction accuracy higher than the use of individual bands. Soil moisture indirectly affects vegetation canopy water content. Red edge and SWIR are the most important spectral bands [72]. The Red Edge 3 and the SWIR 1 bands play an important role in estimating canopy water content [73]. Thus, these bands can better retrieve soil moisture over vegetation-covered areas than other bands. Thus, this is what we concluded from this research paper.

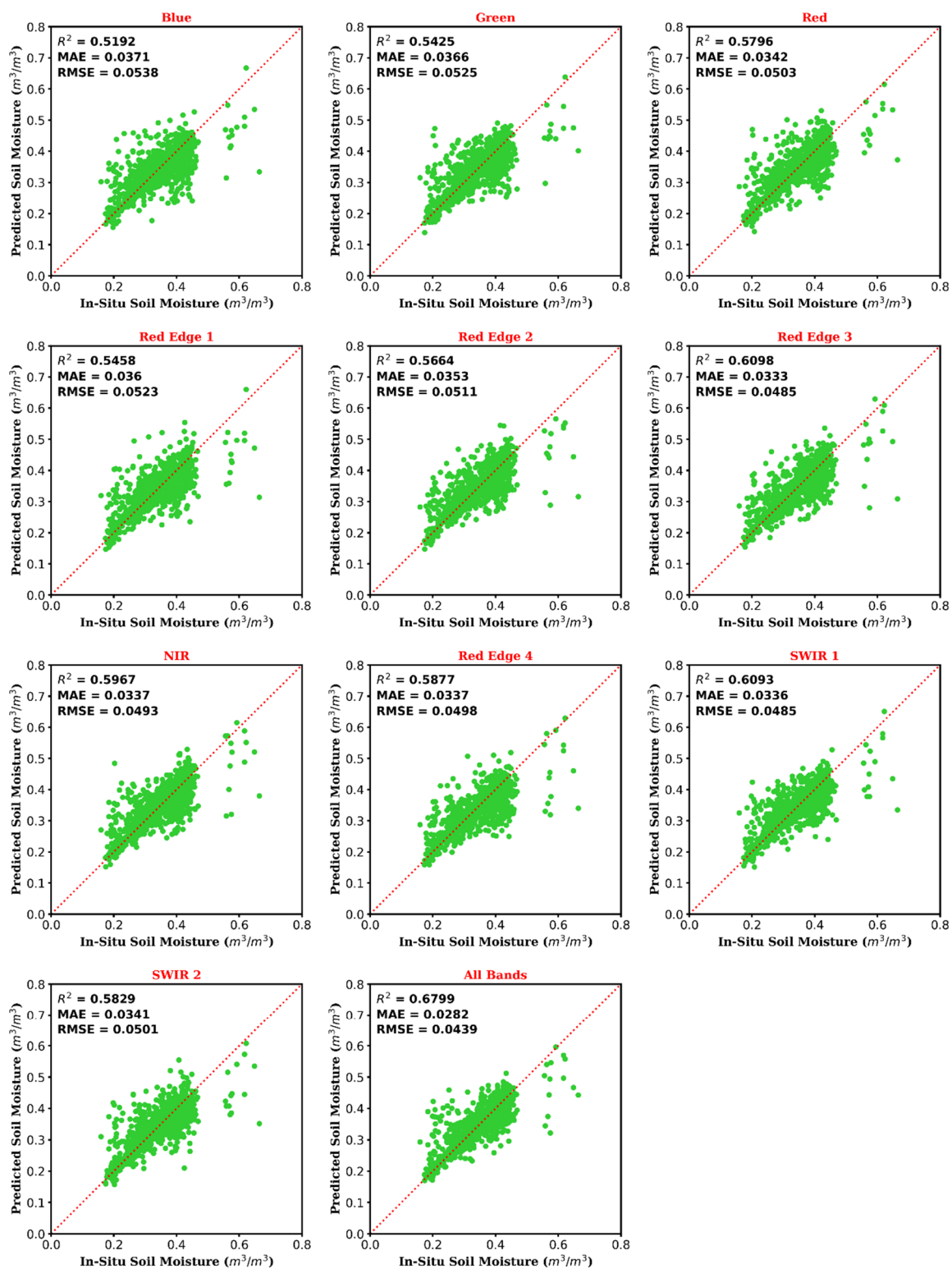
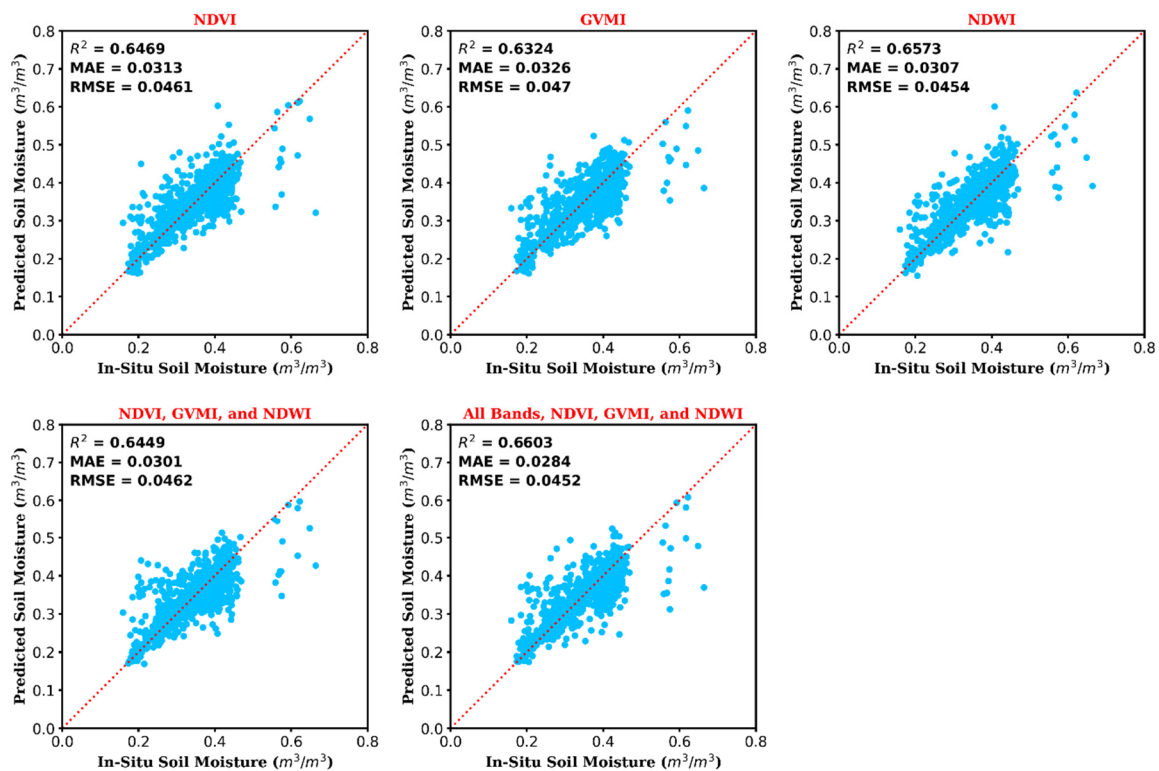


Figure 3. Results of using Sentinel-2 bands as input data to the CNN architecture (3).

### 3.2. Influence of Using NDVI, GVMI, and NDWI

Figure 4 illustrates the findings of using indicators as input data for CNN architecture (3) on the retrieval accuracy of soil moisture. The best indicators for soil moisture retrieval were NDWI ( $R^2 = 0.6573$ ), followed by NDVI ( $R^2 = 0.6469$ ), and then GVMI ( $R^2 = 0.6324$ ). Compared to NDWI, there was a slight decline in the values of the performance metrics ( $R^2 = 0.6449$ , MAE = 0.0301, RMSE = 0.0462) with the use of all

indicators as input data to CNN architecture (3). Further, there was a decrease in the values of the performance metrics from ( $R^2 = 0.6799$ ,  $MAE = 0.0282$ ,  $RMSE = 0.0439$ ) to ( $R^2 = 0.6603$ ,  $MAE = 0.0284$ ,  $RMSE = 0.0452$ ) due to using both Sentinel-2 bands (10 bands) and indicators (three indicators) instead of using all Sentinel-2 bands (10 bands) as input data for the CNN architecture (3). An explanation for this decrease is that the accuracy of the CNN algorithm depends on the quality of the input data. Appropriate features increase accuracy [74]. Repeated features negatively affect the efficiency of the CNN algorithm [75]. These indicators were derived from the original bands. Thus, when using both indicators and bands together as input data to a CNN model, these indicators can be considered a form of repetition to bands indirectly.



**Figure 4.** Results of using NDVI, GVMI, and NDWI as input data to the CNN architecture (3).

The obtained results indicated that the indicator (NDWI, NDVI, or GVMI) is better than the original or single Sentinel-2 band as input data to CNN architecture for soil moisture retrieval. This result is when the input data is a single input (either a band or an indicator). This is because the indicator is usually designed by combining two or more bands. Therefore, it may contain more information than a band. This result is dissimilar to the finding of [72], who stated that by the random forest regression algorithm, the use of the original Sentinel-2 band achieved higher prediction accuracy than the use of the indicator. However, using all Sentinel-2 bands (10 inputs) is more proper than indicators as input data for CNN for retrieving moisture in the soil.

### 3.3. Influence of Using Combinations

Our above results demonstrated that the more information the input layer contains, the better the accuracy of soil moisture retrieval. The indicator, which merges two or more bands, was better than the single band. Further, using all Sentinel-2 bands was the best. We created six new combinations of Sentinel-2 bands to study the integrations between different Sentinel-2 bands and determine the best inputs among them. These combinations were created based on the results of using the single Sentinel-2 bands as input data to the CNN architecture (3).

The first combination consisted of the Green, Red, and NIR bands (top three 10-m bands). The second combination consisted of the Red Edge 3, Red Edge 4, and SWIR 1 bands (top three 20-m bands). The third combination consisted of the NIR, SWIR 1, and SWIR 2 bands (According to [40–45]). The fourth combination consisted of the Green, Red, NIR, SWIR 1, and SWIR 2 bands (top three 10-m bands and SWIR bands). The fifth combination consisted of the Red Edge 3, NIR, Red Edge 4, and SWIR 1 bands (best four bands in this paper). The sixth combination consisted of the Red, Red Edge 1, Red Edge 2, Red Edge 3, NIR, and Red Edge 4 bands (According to [25,29,37,46]).

Figure 5 shows the results of using combinations inferred. Changing the number of Sentinel-2 bands used as input data to CNN architecture (3) influenced the prediction accuracy. The values of the performance metrics were significantly improved by using these combinations. The values of the performance metrics reached ( $R^2 = 0.6344$ , MAE = 0.0301, RMSE = 0.0469), ( $R^2 = 0.6491$ , MAE = 0.0297, RMSE = 0.046), ( $R^2 = 0.6661$ , MAE = 0.0294, RMSE = 0.0448), ( $R^2 = 0.6847$ , MAE = 0.0282, RMSE = 0.0436), ( $R^2 = 0.7015$ , MAE = 0.0287, RMSE = 0.0424), and ( $R^2 = 0.7094$ , MAE = 0.0277, RMSE = 0.0418) for the first, second, third, fourth, fifth, and sixth combinations, respectively.

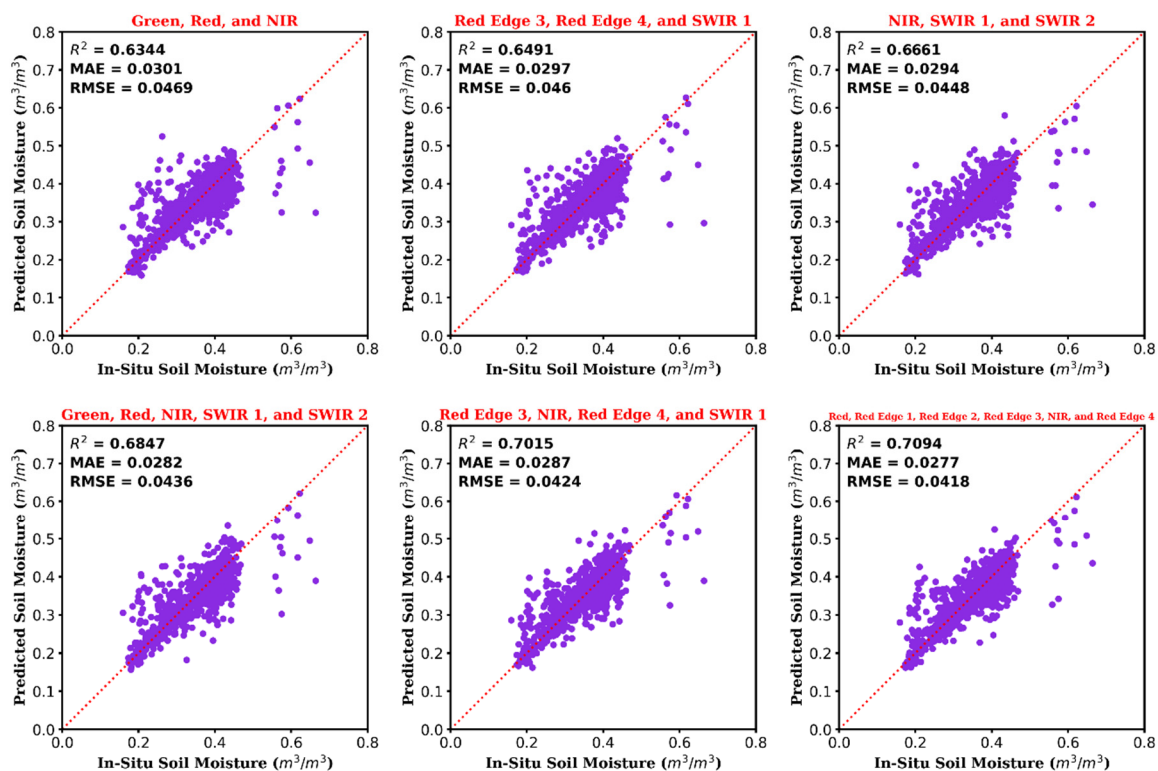


**Figure 5.** Results of using combinations inferred as input data to the CNN architecture (3).

The results indicate that bands at 20 m spatial resolution are better than bands at 10 m spatial resolution. Merging NIR and SWIR bands increased the accuracy of soil moisture retrieval. This result is consistent with the results of [40,45]. Combining SWIR bands with bands at 10 m spatial resolution improved this result from ( $R^2 = 0.6344$ , MAE = 0.0301, RMSE = 0.0469) to ( $R^2 = 0.6847$ , MAE = 0.0282, RMSE = 0.0436). The integration of Red Edge 3, NIR, Red Edge 4, and SWIR 1 bands positively affected soil moisture retrieval accuracy. Combining the Red, NIR, and Red Edge bands was successful and even achieved the highest accuracy of soil moisture retrieval from Sentinel-2 images. In our view, we believe that the main reason for the success of the sixth combination is the addition of the Red Edge bands. The Red Edge bands are suitable and significant for estimating biophysical parameters [76–80]. Biophysical parameters are an indicator of the

status and health of the plant. Therefore, in vegetation-covered areas, Red Edge bands can improve soil moisture retrieval accuracy. This result is similar to the findings of [37].

We conclude from the above reported results that selecting specific bands and using them as input data for the CNN model is better than using indicators or a single Sentinel-2 band and also is better than using all Sentinel-2 bands at once. This result is consistent with the observations of [19]. The perfect three inputs for the CNN architecture (3) are the fourth combination, the fifth combination, and the sixth combination.

### 3.4. Comparison of Different CNN Architectures

As pointed out earlier, we used three CNN architectures (CNN architecture (1), CNN architecture (2), and CNN architecture (3)) of different sizes (Figure 2). Further, to select the best CNN architecture in terms of size, we used the best three inputs (the fourth combination, the fifth combination, and the sixth combination) as input data to the three CNN architectures (1, 2, and 3).

Table 2 summarizes the impact of different CNN architectures on the prediction accuracy. The prediction accuracy of the CNN architecture was negatively affected by the decrease in the number of convolutional layers or/and also the number of filters in a convolution layer. As a result of using the CNN architecture (1), there was a significant reduction in performance metrics from ( $R^2 = 0.6847$ , MAE = 0.0282, RMSE = 0.0436), ( $R^2 = 0.7015$ , MAE = 0.0287, RMSE = 0.0424), and ( $R^2 = 0.7094$ , MAE = 0.0277, RMSE = 0.0418) to ( $R^2 = 0.5999$ , MAE = 0.0335, RMSE = 0.0491), ( $R^2 = 0.6123$ , MAE = 0.0332, RMSE = 0.0483), and ( $R^2 = 0.6128$ , MAE = 0.033, RMSE = 0.0483) for the fourth, fifth, and sixth combinations, respectively. While the use of the CNN architecture (2) caused a decline in the values of the performance metrics to ( $R^2 = 0.6541$ , MAE = 0.0291, RMSE = 0.0456), ( $R^2 = 0.67$ , MAE = 0.0289, RMSE = 0.0446), and ( $R^2 = 0.6706$ , MAE = 0.0289, RMSE = 0.0445) for the fourth, fifth, and sixth combinations, respectively. Based on these findings, CNN architecture (3) is the most appropriate architecture in terms of size for Sentinel-2 data.

**Table 2.** Performance metrics of all architectures.

Input Data	Architecture	$R^2$	MAE	RMSE
Fourth Combination Green, Red, NIR, SWIR 1, and SWIR 2 bands	CNN architecture (1)	0.5999	0.0335	0.0491
	CNN architecture (2)	0.6541	0.0291	0.0456
	CNN architecture (3)	0.6847	0.0282	0.0436
Fifth Combination Red Edge 3, NIR, Red Edge 4, and SWIR 1 bands	CNN architecture (1)	0.6123	0.0332	0.0483
	CNN architecture (2)	0.67	0.0289	0.0446
	CNN architecture (3)	0.7015	0.0287	0.0424
Sixth Combination Red, Red Edge 1, Red Edge 2, Red Edge 3, NIR, and Red Edge 4 bands	CNN architecture (1)	0.6128	0.033	0.0483
	CNN architecture (2)	0.6706	0.0289	0.0445
	CNN architecture (3)	0.7094	0.0277	0.0418

These results show that the prediction accuracy is affected by the size of the CNN architecture. The increase in the number of convolution layers and the number of filters in convolutional layers are the main reasons for the superiority of the CNN architecture (3). The depth of the network highly affects the prediction accuracy of the algorithm [81,82]. Experimental results have shown that the number of layers has a significant impact on CNN performance, suggesting that deeper convolutional networks have better overall performance [83,84]. CNN model generally contains a large number of parameters [85]. The significant parameters affecting CNN accuracy are the number of convolution layers [82] and the number of filters in convolutional layers [86]. Increasing the number of filters used increases the accuracy of the algorithm [87].

Ultimately, CNN architecture (3) is the best architecture that fits this type of data. Further, the best inputs for CNN architecture (3) to achieve accurate prediction of soil moisture from Sentinel-2 images are the fourth combination ( $R^2 = 0.6847$ , MAE = 0.0282, RMSE = 0.0436), the fifth combination ( $R^2 = 0.7015$ , MAE = 0.0287, RMSE = 0.0424), and the sixth combination ( $R^2 = 0.7094$ , MAE = 0.0277, RMSE = 0.0418). These results indicate that using CNN is better than using ANN [33] for estimating surface soil moisture from Sentinel data. Sentinel-2 data can be used to estimate surface soil moisture over vegetation-covered areas, and this helps decision-makers in water management.

To evaluate and demonstrate the performance of the proposed CNN model in a continuous period, Figure 6 shows the long-term soil moisture time series derived from the CNN architecture (3) at three stations in three different sites, and the input data is the sixth combination. Three stations were selected, the first station is Kyeamba 12 in a Kyeamba site, the second station is Yanco 04 in a Yanco site, and the third station is WegenerNet 78 in a WegenerNet site. The available input data for the selected Kyeamba 12 and Yanco 04 stations were started in December 2018, while the available input data for the selected WegenerNet 78 were started in March 2017.

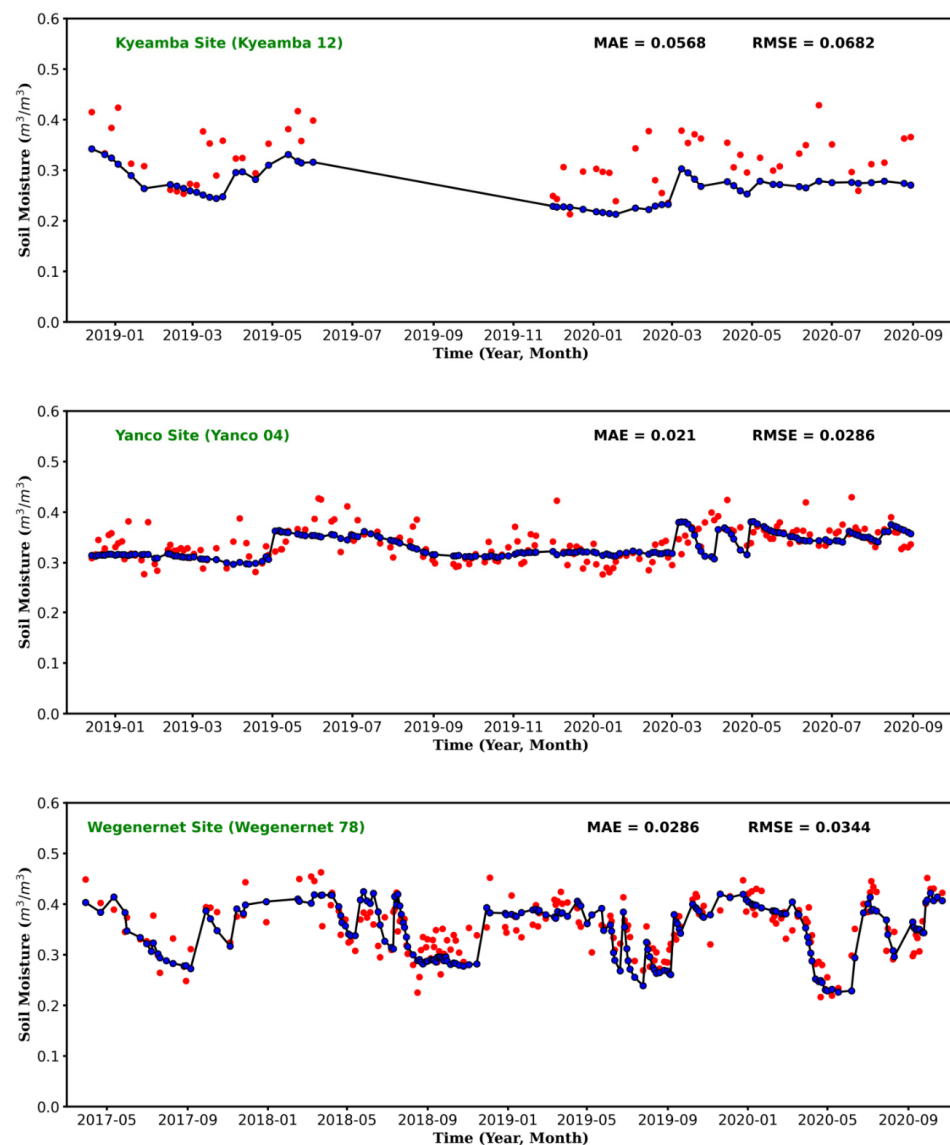


**Figure 6.** Soil moisture time series derived from the CNN architecture (3) for three locations. The black line with the blue points is in-situ soil moisture, and the red points are predicted soil moisture by the proposed CNN algorithm.

From Figure 6, we conclude that the proposed algorithm has succeeded in predicting long-term soil moisture. The results obtained using the sixth combination as input data for CNN architecture (3) were (MAE = 0.0568, RMSE = 0.0682) at Kyeamba 12, (MAE = 0.021, RMSE = 0.0286) at Yanco 04, and (MAE = 0.0286, RMSE = 0.0344) at We-generNet 78. The reported results in the figure indicate that the algorithm is less sensitive to low soil moisture. This is the reason for the high values (MAE and RMSE) at Kyeamba 12, as most of the soil moisture values at the Kyeamba 12 site are less than ( $0.28 \text{ m}^3/\text{m}^3$ ). The main reason for this is that the number of soil moisture data at low values was not enough. Therefore, we anticipate that increasing the amount of soil moisture data at low values will help to increase the algorithm's sensitivity to low soil moisture.

#### 4. Conclusions

Water is central, sacred, and vital to all life. Agriculture is the prime source of food for all living organisms but is considered the main and the biggest user of freshwater. Further, smart agriculture is a major key player in achieving food and water security for the world population. Satellites and artificial intelligence are among the available technologies that can help to achieve smart agriculture. Soil moisture estimation is the first step required to implement smart irrigation in agriculture. Accurate soil moisture estimates help determine the proper timing and amount of irrigation.

We aim, in this paper, to integrate artificial intelligence techniques and Sentinel-2 imagery data to provide a new approach for determining soil moisture without actual contact with soil and in a short time. We propose a CNN architecture for predicting soil moisture over vegetation-covered areas from Sentinel-2 images. The results of this study indicate that CNN architecture (3) is the most suitable architecture. Output always depends on the input. The best inputs to the proposed CNN algorithm for soil moisture retrieval from Sentinel-2 images are the sixth combination composed of the Red, Red Edge 1, Red Edge 2, Red Edge 3, NIR, and Red Edge 4 bands; followed by the fifth combination composed of the Red Edge 3, NIR, Red Edge 4, and SWIR 1 bands; and then the fourth combination composed of the Green, Red, NIR, SWIR 1, and SWIR 2 bands. Using the sixth combination as input data to the CNN architecture (3) achieved the best values of the performance metrics ( $R^2 = 0.7094$ , MAE = 0.0277, RMSE = 0.0418). Results also show that both Red Edge 3 and SWIR 1 bands are considered more sensitive than the other Sentinel-2 bands for estimating soil moisture. Furthermore, the NDWI is more sensitive than NDVI and GVMi. Using the combinations "that consist of some number of Sentinel-2 bands" as input data for CNN architecture is better than using each band separately or all of them at once and is also better than the use of indicators either separately or in combination. Eventually, we need to use two- or three-times the number of Sentinel-2 images used in this research to improve this algorithm and obtain accurate measurements from the CNN model for the precision of field measurements. We will seek to illustrate and prove this in future research.

**Author Contributions:** Conceptualization, E.H.H. and J.H.; methodology, E.H.H.; Sentinel-2 data pre-processing, E.H.H. and L.Y.; data curation, E.H.H.; software, E.H.H.; validation, E.H.H., A.A.S. and R.H.; formal analysis, E.H.H.; investigation, E.H.H., A.A.S. and J.H.; writing—original draft, E.H.H.; writing—review and editing, E.H.H., A.A.S., L.Y., R.H. and J.H.; supervision, J.H. All authors have read and agreed to the published version of the manuscript.

**Funding:** This research was funded by The Project Supported by the Key R&D Program of Zhejiang Province (2021C02036), a scholarship (2018GBJ008523) under the joint program (Executive Program between the Arab Republic of Egypt and P.R of China), and the Erasmus+ Project (598838-EPP-1-2018-EL-EPPKA2-CBHE-JP).

**Institutional Review Board Statement:** Not applicable.

**Informed Consent Statement:** Not applicable.

**Data Availability Statement:** The data presented in this study are available on request from the corresponding author.

**Acknowledgments:** The authors express their sincere gratitude to the data providers and the International Soil Moisture Network (ISMN) for the OzNet and WegenerNet data.

**Conflicts of Interest:** The authors declare no conflict of interest.

## References

1. United Nations Department of Economic and Social Affairs (DESA), Population Division. *World Population Prospects: The 2015 Revision, Key Findings and Advance Tables*; Working Paper No. ESA/P/WP.241; Department of Economic and Social Affairs, Population Division: New York, NY, USA, 2015; pp. 1–66.
2. FAO. *Agriculture, Food, and Water: A Contribution to the World Water Development Report*; FAO: Rome, Italy, 2003; p. 64.
3. Alexandratos, N.; Bruinsma, J. *World Agriculture Towards 2030/2050: The 2012 Revision*; ESA Working Paper No. 12-03; Food and Agriculture Organization of the United Nations, Agricultural Development Economics Division (ESA): Rome, Italy, 2012; p. 154.
4. FAO. *The Future of Food and Agriculture—Trends and Challenges*; FAO: Rome, Italy, 2017; p. 296.
5. Jain, S.K.; Singh, V.P. *Water Resources Systems Planning and Management*; Elsevier: Amsterdam, The Netherlands, 2003.
6. Ray, D.K.; West, P.C.; Clark, M.; Gerber, J.S.; Prishchepov, A.V.; Chatterjee, S. Climate Change Has Likely Already Affected Global Food Production. *PLoS ONE* **2019**, *14*, e0217148. [[CrossRef](#)] [[PubMed](#)]
7. Strzepek, K.; Boehlert, B. Competition for Water for the Food System. *Philos. Trans. R. Soc. B Biol. Sci.* **2010**, *365*, 2927–2940. [[CrossRef](#)] [[PubMed](#)]
8. FAO. *The State of the World's Land and Water Resources for Food and Agriculture (SOLAW)—Managing Systems at Risk*; Food and Agriculture Organization of the United Nations: Rome, Italy; Earthscan: London, UK, 2011.
9. Dabach, S.; Lazarovitch, N.; Šimůnek, J.; Shani, U. Numerical Investigation of Irrigation Scheduling Based on Soil Water Status. *Irrig. Sci.* **2013**, *31*, 27–36. [[CrossRef](#)]
10. Jimenez, A.-F.; Cardenas, P.-F.; Jimenez, F.; Canales, A.; López, A. A Cyber-Physical Intelligent Agent for Irrigation Scheduling in Horticultural Crops. *Comput. Electron. Agric.* **2020**, *178*, 105777. [[CrossRef](#)]
11. Ihuoma, S.O.; Madramootoo, C.A. Recent Advances In Crop Water Stress Detection. *Comput. Electron. Agric.* **2017**, *141*, 267–275. [[CrossRef](#)]
12. Romano, N. Soil Moisture at Local Scale: Measurements and Simulations. *J. Hydrol.* **2014**, *516*, 6–20. [[CrossRef](#)]
13. Halloran, L.J.S.; Rau, G.C.; Andersen, M.S. Heat as A Tracer to Quantify Processes and Properties in the Vadose Zone: A Review. *Earth-Sci. Rev.* **2016**, *159*, 358–373. [[CrossRef](#)]
14. Entekhabi, D.; Njoku, E.G.; O'Neill, P.E.; Kellogg, K.H.; Crow, W.T.; Edelstein, W.N.; Entin, J.K.; Goodman, S.D.; Jackson, T.J.; Johnson, J.; et al. The Soil Moisture Active Passive (SMAP) Mission. *Proc. IEEE* **2010**, *98*, 704–716. [[CrossRef](#)]
15. Mohamed, E.S.; Ali, A.; El-Shirbeny, M.; Abutaleb, K.; Shaddad, S.M. Mapping Soil Moisture and their Correlation with Crop Pattern Using Remotely Sensed Data in Arid Region. *Egypt. J. Remote Sens. Space Sci.* **2020**, *23*, 347–353. [[CrossRef](#)]
16. Liang, S.; Wang, J. *Advanced Remote Sensing: Terrestrial Information Extraction and Applications*, 2nd ed.; Academic Press: London, UK, 2020.
17. Babaeian, E.; Sadeghi, M.; Jones, S.B.; Montzka, C.; Vereecken, H.; Tuller, M. Ground, Proximal, and Satellite Remote Sensing of Soil Moisture. *Rev. Geophys.* **2019**, *57*, 530–616. [[CrossRef](#)]
18. Verstraeten, W.W.; Veroustraete, F.; Feyen, J. Assessment of Evapotranspiration and Soil Moisture Content Across Different Scales of Observation. *Sensors* **2008**, *8*, 70–117. [[CrossRef](#)] [[PubMed](#)]
19. Hegazi, E.H.; Yang, L.; Huang, J. A Convolutional Neural Network Algorithm for Soil Moisture Prediction from Sentinel-1 SAR Images. *Remote Sens.* **2021**, *13*, 4964. [[CrossRef](#)]
20. Wang, L.; Qu, J.J. Satellite Remote Sensing Applications for Surface Soil Moisture Monitoring: A Review. *Front. Earth Sci. China* **2009**, *3*, 237–247. [[CrossRef](#)]
21. Sadeghi, M.; Jones, S.B.; Philpot, W.D. A Linear Physically-Based Model for Remote Sensing of Soil Moisture Using Short Wave Infrared Bands. *Remote Sens. Environ.* **2015**, *164*, 66–76. [[CrossRef](#)]
22. Ångström, A. The Albedo of Various Surfaces of Ground. *Geogr. Ann.* **1925**, *7*, 323–342. [[CrossRef](#)]
23. Chen, M.; Zhang, Y.; Yao, Y.; Lu, J.; Pu, X.; Hu, T.; Wang, P. Evaluation of the OPTRAM Model to Retrieve Soil Moisture in the Sanjiang Plain of Northeast China. *Earth Space Sci.* **2020**, *7*, e2020EA001108. [[CrossRef](#)]
24. Wang, H.; Li, X.; Long, H.; Xu, X.; Bao, Y. Monitoring the Effects of Land Use and Cover Type Changes on Soil Moisture Using Remote-Sensing Data: A Case Study in China's Yongding River Basin. *Catena* **2010**, *82*, 135–145. [[CrossRef](#)]
25. Amani, M.; Parsian, S.; MirMazloumi, S.M.; Aieneh, O. Two New Soil Moisture Indices Based on the NIR-Red triangle Space of Landsat-8 Data. *Int. J. Appl. Earth Obs. Geoinf.* **2016**, *50*, 176–186. [[CrossRef](#)]
26. Hezarian, F.; Khalilimoghadam, B.; Zoratipour, A.; Nejad, M.F.; Yusefi, A. Assessment of the Capability of Satellite Images in Determining the Topsoil Moisture Content in the Dust Hotspot of Southeastern Ahvaz in Iran. *Eurasian Soil Sci.* **2022**, *55*, 1576–1590. [[CrossRef](#)]
27. Lobell, D.B.; Asner, G.P. Moisture Effects on Soil Reflectance. *Soil Sci. Soc. Am. J.* **2002**, *66*, 722–727. [[CrossRef](#)]

28. Yang, X.; Yu, Y.; Li, M. Estimating Soil Moisture Content Using Laboratory Spectral Data. *J. For. Res.* **2019**, *30*, 1073–1080. [[CrossRef](#)]
29. Hashim, B.M.; Sultan, M.A.; Attyia, M.N.; Al Maliki, A.A.; Al-Ansari, N. Change Detection and Impact of Climate Changes to Iraqi Southern Marshes Using Landsat 2 MSS, Landsat 8 OLI and Sentinel 2 MSI Data and GIS Applications. *Appl. Sci.* **2019**, *9*, 2016. [[CrossRef](#)]
30. Sanchez, N.; Alonso-Arroyo, A.; Martínez-Fernández, J.; Camps, A.; González-Zamora, A.; Pablos, M.; Herrero-Jiménez, C.M.; Gumuzzio, A. Multisensor Experiments Over Vineyard: New Challenges for the Gns-R Technique. In Proceedings of the ISPRS International Archives of the Photogrammetry, Remote Sensing and Spatial Information Sciences: 36th International Symposium on Remote Sensing of Environment, Berlin, Germany, 11–15 May 2015.
31. Ambrosone, M.; Matese, A.; Di Gennaro, S.F.; Gioli, B.; Tudoroiu, M.; Genesisio, L.; Miglietta, F.; Baronti, S.; Maienza, A.; Ungaro, F.; et al. Retrieving Soil Moisture in Rainfed and Irrigated Fields Using Sentinel-2 Observations and A Modified OPTRAM Approach. *Int. J. Appl. Earth Obs. Geoinf.* **2020**, *89*, 102113. [[CrossRef](#)]
32. Ma, C.; Li, X.; McCabe, M.F. Retrieval of High-Resolution Soil Moisture through Combination of Sentinel-1 and Sentinel-2 Data. *Remote Sens.* **2020**, *12*, 2303. [[CrossRef](#)]
33. Nativel, S.; Ayari, E.; Rodriguez-Fernandez, N.; Baghdadi, N.; Madelon, R.; Albergel, C.; Zribi, M. Hybrid Methodology Using Sentinel-1/Sentinel-2 for Soil Moisture Estimation. *Remote Sens.* **2022**, *14*, 2434. [[CrossRef](#)]
34. Wang, Q.; Li, J.; Jin, T.; Chang, X.; Zhu, Y.; Li, Y.; Sun, J.; Li, D. Comparative Analysis of Landsat-8, Sentinel-2, and GF-1 Data for Retrieving Soil Moisture over Wheat Farmlands. *Remote Sens.* **2020**, *12*, 2708. [[CrossRef](#)]
35. Gangat, R.; Van Deventer, H.; Naidoo, L.; Adam, E. Estimating Soil Moisture Using Sentinel-1 and Sentinel-2 Sensors for Dryland and Palustrine Wetland Areas. *South Afr. J. Sci.* **2020**, *116*, 1–9. [[CrossRef](#)]
36. Zheng, X.; Feng, Z.; Li, L.; Li, B.; Jiang, T.; Li, X.; Li, X.; Chen, S. Simultaneously Estimating Surface Soil Moisture and Roughness of Bare Soils by Combining Optical and Radar Data. *Int. J. Appl. Earth Obs. Geoinf.* **2021**, *100*, 102345. [[CrossRef](#)]
37. Liu, Y.; Qian, J.; Yue, H. Comprehensive Evaluation of Sentinel-2 Red Edge and Shortwave-Infrared Bands to Estimate Soil Moisture. *IEEE J. Sel. Top. Appl. Earth Obs. Remote Sens.* **2021**, *14*, 7448–7465. [[CrossRef](#)]
38. Jackson, T.J.; Chen, D.; Cosh, M.; Li, F.; Anderson, M.; Walthall, C.; Doriaswamy, P.; Hunt, E.R. Vegetation Water Content Mapping Using Landsat Data Derived Normalized Difference Water Index for Corn and Soybeans. *Remote Sens. Environ.* **2004**, *92*, 475–482. [[CrossRef](#)]
39. Yilmaz, M.T.; Hunt Jr, E.R.; Jackson, T.J. Remote Sensing of Vegetation Water Content from Equivalent Water Thickness using Satellite Imagery. *Remote Sens. Environ.* **2008**, *112*, 2514–2522. [[CrossRef](#)]
40. Wang, Q.; Jin, T.; Li, J.; Chang, X.; Li, Y.; Zhu, Y. Modeling and Assessment of Vegetation Water Content on Soil Moisture Retrieval via the Synergistic Use of Sentinel-1 and Sentinel-2. *Earth Space Sci.* **2022**, *9*, e2021EA002063. [[CrossRef](#)]
41. Ceccato, P.; Gobron, N.; Flasse, S.; Pinty, B.; Tarantola, S. Designing A Spectral Index to Estimate Vegetation Water Content from Remote Sensing Data: Part 1: Theoretical Approach. *Remote Sens. Environ.* **2002**, *82*, 188–197. [[CrossRef](#)]
42. Gao, B.-C. NDWI—A Normalized Difference Water Index for Remote Sensing of Vegetation Liquid Water from Space. *Remote Sens. Environ.* **1996**, *58*, 257–266. [[CrossRef](#)]
43. Holtgrave, A.-K.; Röder, N.; Ackermann, A.; Erasmi, S.; Kleinschmit, B. Comparing Sentinel-1 and-2 Data and Indices for Agricultural Land Use Monitoring. *Remote Sens.* **2020**, *12*, 2919. [[CrossRef](#)]
44. Sun, H.; Liu, H.; Ma, Y.; Xia, Q. Optical Remote Sensing Indexes of Soil Moisture: Evaluation and Improvement Based on Aircraft Experiment Observations. *Remote Sens.* **2021**, *13*, 4638. [[CrossRef](#)]
45. Wang, Q.; Li, P.; Pu, Z.; Chen, X. Calibration and Validation of Salt-Resistant Hyperspectral Indices for Estimating Soil Moisture in Arid Land. *J. Hydrol.* **2011**, *408*, 276–285. [[CrossRef](#)]
46. Zhan, Z.; Qin, Q.; Ghulan, A.; Wang, D. NIR-Red Spectral Space Based New Method for Soil Moisture Monitoring. *Sci. China Ser. D: Earth Sci.* **2007**, *50*, 283–289. [[CrossRef](#)]
47. Gorelick, N.; Hancher, M.; Dixon, M.; Ilyushchenko, S.; Thau, D.; Moore, R. Google Earth Engine: Planetary-Scale Geospatial Analysis for Everyone. *Remote Sens. Environ.* **2017**, *202*, 18–27. [[CrossRef](#)]
48. You, N.; Dong, J. Examining Earliest Identifiable Timing of Crops Using All Available Sentinel 1/2 Imagery and Google Earth Engine. *ISPRS J. Photogramm. Remote Sens.* **2020**, *161*, 109–123. [[CrossRef](#)]
49. Krittanawong, C.; Zhang, H.; Wang, Z.; Aydar, M.; Kitai, T. Artificial Intelligence in Precision Cardiovascular Medicine. *J. Am. Coll. Cardiol.* **2017**, *69*, 2657–2664. [[CrossRef](#)] [[PubMed](#)]
50. Hardian, R.; Liang, Z.; Zhang, X.; Szekely, G. Artificial Intelligence: The Silver Bullet for Sustainable Materials Development. *Green Chem.* **2020**, *22*, 7521–7528. [[CrossRef](#)]
51. Müller, A.C.; Guido, S. *Introduction to Machine Learning with Python: A Guide for Data Scientists*, 1st ed.; O'Reilly Media, Inc.: Sebastopol, CA, USA, 2016.
52. Alpaydin, E. *Introduction to Machine Learning*, 3rd ed.; MIT Press: Cambridge, MA, USA, 2014.
53. LeCun, Y.; Bengio, Y.; Hinton, G. Deep Learning. *Nature* **2015**, *521*, 436–444. [[CrossRef](#)]
54. Yamashita, R.; Nishio, M.; Do, R.K.G.; Togashi, K. Convolutional Neural Networks: An Overview and Application in Radiology. *Insights Into Imaging* **2018**, *9*, 611–629. [[CrossRef](#)]
55. Lee, C.; Panda, P.; Srinivasan, G.; Roy, K. Training Deep Spiking Convolutional Neural Networks With STDP-Based Unsupervised Pre-training Followed by Supervised Fine-Tuning. *Front. Neurosci.* **2018**, *12*, 435. [[CrossRef](#)] [[PubMed](#)]

56. Zhu, M.; Ye, K.; Xu, C.-Z. Network Anomaly Detection and Identification Based on Deep Learning Methods. In Proceedings of the International Conference on Cloud Computing, Cloud Computing—CLOUD 2018, CLOUD 2018, Lecture Notes in Computer Science, Seattle, WA, USA, 25–30 June 2018; pp. 219–234.
57. Galib, S.M. Applications of Machine Learning in Nuclear Imaging and Radiation Detection. Ph.D. Thesis, Missouri University of Science and Technology, Rolla, MO, USA, 2019.
58. Chen, Z.; Gryllias, K.; Li, W. Mechanical Fault Diagnosis Using Convolutional Neural Networks and Extreme Learning Machine. *Mech. Syst. Signal Process.* **2019**, *133*, 106272. [CrossRef]
59. Dorigo, W.A.; Wagner, W.; Hohensinn, R.; Hahn, S.; Paulik, C.; Xaver, A.; Gruber, A.; Drusch, M.; Mecklenburg, S.; van Oevelen, P.; et al. International Soil Moisture Network: A Data Hosting Facility for Global In Situ Soil Moisture Measurements. *Hydrol. Earth Syst. Sci.* **2011**, *15*, 1675–1698. [CrossRef]
60. Dorigo, W.A.; Xaver, A.; Vreugdenhil, M.; Gruber, A.; Hegyiova, A.; Sanchis-Dufau, A.D.; Zamojski, D.; Cordes, C.; Wagner, W.; Drusch, M. Global Automated Quality Control of In Situ Soil Moisture Data from the International Soil Moisture Network. *Vadose Zone J.* **2013**, *12*, 1–21. [CrossRef]
61. Smith, A.B.; Walker, J.P.; Western, A.W.; Young, R.I.; Ellett, K.M.; Pipunic, R.C.; Grayson, R.B.; Siriwardena, L.; Chiew, F.H.S.; Richter, H. The Murrumbidgee Soil Moisture Monitoring Network Data Set. *Water Resour. Res.* **2012**, *48*, 1–6. [CrossRef]
62. Young, R.; Walker, J.; Yeoh, N.; Smith, A.; Ellett, K.; Merlin, O.; Western, A. *Soil Moisture and Meteorological Observations from the Murrumbidgee Catchment*; Department of Civil and Environmental Engineering, The University of Melbourne: Melbourne, VIC, Australia, 2008; p. 54.
63. Fuchsberger, J.; Kirchengast, G.; Kabas, T. WegenerNet High-Resolution Weather and Climate Data from 2007 to 2020. *Earth Syst. Sci. Data* **2021**, *13*, 1307–1334. [CrossRef]
64. Kabas, T. WegenerNet Klimastationsnetz Region Feldbach: Experimenteller Aufbau und hochauflösende Daten für die Klima- und Umweltforschung. Ph.D. Thesis, University of Graz, Graz, Austria, 2011.
65. Kirchengast, G.; Kabas, T.; Leuprecht, A.; Bichler, C.; Truhetz, H. WegenerNet: A Pioneering High-Resolution Network for Monitoring Weather and Climate. *Bull. Am. Meteorol. Soc.* **2014**, *95*, 227–242. [CrossRef]
66. Drusch, M.; Del Bello, U.; Carlier, S.; Colin, O.; Fernandez, V.; Gascon, F.; Hoersch, B.; Isola, C.; Laberinti, P.; Martimort, P.; et al. Sentinel-2: ESA's Optical High-Resolution Mission for GMES Operational Services. *Remote Sens. Environ.* **2012**, *120*, 25–36. [CrossRef]
67. Louis, J.; Devignot, O.; Pessiot, L. *S2 MPC-L2A Product Definition Document*; Ref. S2-PDGS-MPC-L2A-PDD-V14.5. 2018. Available online: <http://step.esa.int/thirdparties/sen2cor/2.5.5/docs/S2-PDGS-MPC-L2A-PDD-V2.5.5.pdf> (accessed on 13 November 2020).
68. Main-Knorn, M.; Pflug, B.; Louis, J.; Debaecker, V.; Müller-Wilm, U.; Gascon, F. Sen2Cor for Sentinel-2. In Proceedings of the Image and Signal Processing for Remote Sensing XXIII, Warsaw, Poland, 4 October 2017; p. 1042704.
69. Khan, S.; Rahmani, H.; Shah, S.A.A.; Bennamoun, M. A Guide to Convolutional Neural Networks for Computer Vision. In *Synthesis Lectures on Computer Vision*; Morgan & Claypool: San Rafael, CA, USA, 2018; Volume 8, pp. 1–207.
70. Sewak, M.; Karim, M.R.; Pujari, P. *Practical Convolutional Neural Networks: Implement Advanced Deep Learning Models Using Python*; Packt Publishing Ltd.: Birmingham, UK, 2018.
71. Sadeghi, M.; Babaeian, E.; Tuller, M.; Jones, S.B. The Optical Trapezoid Model: A Novel Approach to Remote Sensing of Soil Moisture Applied to Sentinel-2 and Landsat-8 Observations. *Remote Sens. Environ.* **2017**, *198*, 52–68. [CrossRef]
72. Lin, Y.; Zhu, Z.; Guo, W.; Sun, Y.; Yang, X.; Kovalskyy, V. Continuous Monitoring of Cotton Stem Water Potential using Sentinel-2 Imagery. *Remote Sens.* **2020**, *12*, 1176. [CrossRef]
73. Pan, H.; Chen, Z.; Ren, J.; Li, H.; Wu, S. Modeling Winter Wheat Leaf Area Index and Canopy Water Content with Three Different Approaches Using Sentinel-2 Multispectral Instrument Data. *IEEE J. Sel. Top. Appl. Earth Obs. Remote Sens.* **2018**, *12*, 482–492. [CrossRef]
74. Pristyanto, Y.; Adi, S.; Sunyoto, A. The effect of feature selection on classification algorithms in credit approval. In Proceedings of the 2019 International Conference on Information and Communications Technology (ICOIACT), Yogyakarta, Indonesia, 24–25 July 2019; pp. 451–456.
75. Zhang, L.; Chen, J.; Ma, J.; Liu, H. HN-CNN: A Heterogeneous Network Based on Convolutional Neural Network for m7 G Site Disease Association Prediction. *Front. Genet.* **2021**, *12*, 655284. [CrossRef] [PubMed]
76. Clevers, J.G.; Gitelson, A.A. Remote Estimation of Crop and Grass Chlorophyll and Nitrogen Content using Red-Edge Bands on Sentinel-2 and -3. *Int. J. Appl. Earth Obs. Geoinf.* **2013**, *23*, 344–351. [CrossRef]
77. Dash, J.; Curran, P.J. The MERIS Terrestrial Chlorophyll Index. *Int. J. Remote Sens.* **2004**, *25*, 5403–5413. [CrossRef]
78. Delegido, J.; Verrelst, J.; Alonso, L.; Moreno, J. Evaluation of Sentinel-2 Red-Edge Bands for Empirical Estimation of Green LAI and Chlorophyll Content. *Sensors* **2011**, *11*, 7063–7081. [CrossRef]
79. Gitelson, A.A.; Viña, A.; Ciganda, V.; Rundquist, D.C.; Arkebauer, T.J. Remote Estimation of Canopy Chlorophyll Content in Crops. *Geophys. Res. Lett.* **2005**, *32*, L08403. [CrossRef]
80. Xu, N.; Tian, J.; Tian, Q.; Xu, K.; Tang, S. Analysis of Vegetation Red Edge with Different Illuminated/Shaded Canopy Proportions and to Construct Normalized Difference Canopy Shadow Index. *Remote Sens.* **2019**, *11*, 1192. [CrossRef]
81. Nevavuori, P.; Narra, N.; Lipping, T. Crop Yield Prediction with Deep Convolutional Neural Networks. *Comput. Electron. Agric.* **2019**, *163*, 104859. [CrossRef]

82. Özgenel, Ç.F.; Sorguç, A.G. Performance Comparison of Pretrained Convolutional Neural Networks on Crack Detection in Buildings. In Proceedings of the International Symposium on Automation and Robotics in Construction, Berlin, Germany, 20–25 July 2018; pp. 1–8.
83. Emami, H.; Dong, M.; Nejad-Davarani, S.P.; Glide-Hurst, C.K. Generating Synthetic CTs from Magnetic Resonance Images using Generative Adversarial Networks. *Med. Phys.* **2018**, *45*, 3627–3636. [[CrossRef](#)] [[PubMed](#)]
84. Simonyan, K.; Zisserman, A. Very Deep Convolutional Networks for Large-Scale Image Recognition. In Proceedings of the 3rd International Conference on Learning Representations (ICLR 2015), Computational and Biological Learning Society, San Diego, CA, USA, 7–9 May 2015; pp. 1–14.
85. Lu, Y.; Huo, Y.; Yang, Z.; Niu, Y.; Zhao, M.; Bosiakov, S.; Li, L. Influence of the Parameters of the Convolutional Neural Network Model in Predicting the Effective Compressive Modulus of Porous Structure. *Front. Bioeng. Biotechnol.* **2022**, *10*, 1–11. [[CrossRef](#)] [[PubMed](#)]
86. Sameen, M.I.; Pradhan, B.; Lee, S. Application of Convolutional Neural Networks Featuring Bayesian Optimization for Landslide Susceptibility Assessment. *Catena* **2020**, *186*, 104249. [[CrossRef](#)]
87. Ahmed, W.S.; Karim, A.a.A. The Impact of Filter Size and Number of Filters on Classification Accuracy in CNN. In Proceedings of the 2020 International Conference on Computer Science and Software Engineering (CSASE), Duhok, Iraq, 16–18 April 2020; pp. 88–93.

**Disclaimer/Publisher’s Note:** The statements, opinions and data contained in all publications are solely those of the individual author(s) and contributor(s) and not of MDPI and/or the editor(s). MDPI and/or the editor(s) disclaim responsibility for any injury to people or property resulting from any ideas, methods, instructions or products referred to in the content.